Orthogonality catastrophe in ballistic quantum dots: Role of level degeneracies and confinement geometry

Georg Röder and Martina Hentschel
Max-Planck-Institut für Physik komplexer Systeme, Nöthnitzer Str. 38, 01187 Dresden, Germany
(Received 16 April 2010; revised manuscript received 20 July 2010; published 10 September 2010)

We study Anderson orthogonality catastrophe in mesoscopic systems, in particular, in ballistic quantum dots with integrable hard-wall confinement potential. Mesoscopic fluctuations lead to a broad distribution of Anderson many-particle overlaps that we investigate for rectangular, circular, and half-circular quantum dots. We compare our results with those previously obtained for chaotic systems. We find an overall weak dependence of the overlap probability distributions on the system geometry that is, however, more pronounced in the presence of a magnetic field. The existence of level degeneracies, a characteristics of many regular systems, crucially alters the distribution of Anderson overlaps that gain more weight on smaller values. For the twofold degenerate levels of circular quantum dots, we find a double-peak structure of the overlap distribution that we can analytically understand. The double-peak structure disappears gradually as a magnetic control field is switched on. We extent the analytical investigation of this qualitatively new behavior to the general g-fold degenerate case.

DOI: 10.1103/PhysRevB.82.125312 PACS number(s): 73.21.−b, 78.70.Dm, 05.45.Mt, 78.67.−n

I. INTRODUCTION

Many-body effects have been a key interest in condensed-matter physics for several decades. With the increasing versatility in fabricating and measuring mesoscopic and nanoscopic devices, many-body physics in these samples receives growing interest.[1–3] Anderson orthogonality catastrophe (AOC) is a generic many-body effect that arises when a many-electron system responds to a sudden and localized perturbation, such as a suddenly appearing core hole during the x-ray excitation of a core electron. In bulk metals, it refers to the vanishing of the overlap between the many-body ground states before and after the perturbation is applied.[4,5] AOC is one of the many-body responses that lead to Fermi-edge singularities in the x-ray edge problem.[6,7] Orthogonality catastrophe in the mesoscopic regime was studied in the context of parametric random matrices,[8] of finite conductors with disorder[9] as well as for chaotic quantum dots and nanoparticles,[3,10] parabolic quantum dots,[11] and graphene.[12]

In the present paper, we discuss AOC in ballistic mesoscopic systems and compare regular [rectangular and (half)circular] to generic chaotic quantum dots, thereby focusing on a possible geometry dependence of the AOC and the role of level degeneracies. In the mesoscopic case, the finite number of particles generally yields finite, nonvanishing AOC overlaps,[8–10,13] in contrast to the metallic case. The presence of mesoscopic fluctuations leads to a broad distribution of Anderson overlaps that, furthermore, depends on the number of particles in the system. We shall see that the presence of level degeneracies, an specific property of highly symmetric mesoscopic systems, such as the circular and square billiards, that contrasts both the metallic and the generic chaotic case, strongly modifies the overlap distribution: Yet another example that the mesoscopic regime gives rise to qualitatively new behavior, here in AOC physics.

One purpose of this study is to investigate a possible geometry dependence of the AOC response that reflects the dynamical properties of the quantum dot, i.e., regular (integrable) or chaotic dynamics of the classical counterpart of the quantized system. Such a dependence was seen in the weak-localization response in magnetotransport through a circular (regular) and stadium-shaped (chaotic) ballistic quantum dot.[14,15] To this end we discuss the overlap distributions of several regular quantum dot geometries and compare them to the previously studied chaotic case.[10] Whereas we find that overlap distributions of rectangular, half-circular, and generic chaotic quantum dots resemble each other to a large extent, the difference between overlap distributions of circular and generic chaotic quantum dots in the presence of a magnetic field is more pronounced.

The paper is organized as follows. In Sec. II, we introduce ballistic quantum dot model systems: rectangular and (half-) circular quantum billiards, and list their single-particle wave functions and energy spectra. The circular billiards is also treated in the presence of a magnetic field in order to allow one to gradually separate degenerate levels by an external control field. In Sec. III, we introduce the model of a localized, or rank one, potential, describe the calculation of the many-particle overlap and discuss the treatment of twofold degenerate energy levels using the circular billiards as an example. In Sec. IV, we present and compare distributions of Anderson overlaps of regular and chaotic quantum billiards and summarize our results in Sec. V. Finally, an extension of the Anderson overlap treatment in the general case of g-fold degenerate levels is given in Appendix A. A systematic study of mean values of the Anderson overlap in dependence on the system confinement and perturbation strength is included in Appendix B.

II. BRIEF SUMMARY OF INTEGRABLE BALLISTIC QUANTUM DOT MODELS

We consider two-dimensional electronic quantum dots with integrable hard-wall confinement potentials, namely, rectangular, circular, and half-circular billiards as well as circular billiards in the presence of a magnetic field. Except for

the circular billiards with magnetic field that is treated in detail in Ref. 16, the models are discussed in common text books.[17] We summarize single-particle wave functions and energy spectra that solve an effective mass Schrödinger equation for noninteracting spinless electrons.

Rectangular billiards with side lengths L_1 and L_2 are characterized by an aspect ratio $L_1/L_2=\sqrt{\alpha}$. Those with an irrational α possess a nondegenerate energy spectrum. If not otherwise stated, we take α as the Golden ratio, $\alpha=(1+\sqrt{5})/2$. Eigenenergies and eigenfunctions are given by

$$\varepsilon_{n,m} = E_r(n^2 + \alpha m^2), \quad n,m = 1,2,3,\ldots, \tag{1}$$

$$\varphi_{n,m}(x,y) = \frac{2}{\sqrt{L_1 L_2}} \sin\left(n\pi\frac{x}{L_1}\right)\sin\left(m\pi\frac{y}{L_2}\right) \tag{2}$$

with $E_r=\hbar^2\pi^2/(2m^*L_1^2)$ and the effective mass m^*.

In the case of the circular billiards with radius R, the energy eigenvalue problem and the eigenvalue problem of the angular momentum z—component can be solved simultaneously. Energy levels and wave functions, labeled by the angular momentum quantum number $m=0,\pm 1,\pm 2,\ldots$, are

$$\varphi_{m,n}(r,\vartheta) = \frac{1}{\sqrt{2\pi}} e^{im\vartheta} N_{m,n} J_{|m|}\left(\rho_{|m|,n}\frac{r}{R}\right), \tag{3}$$

$$\varepsilon_{m,n} = E_c \rho_{|m|,n}^2 \tag{4}$$

with $E_c=\hbar^2/(2m^*R^2)$ and the normalization constant of the radial wave function $N_{m,n}=\sqrt{2}/[RJ_{|m|+1}(\rho_{|m|,n})]$. The index $n=0,1,2,\ldots$ labels the roots $\rho_{|m|,n}$ of $J_{|m|}$, the Bessel function of the first kind of order $|m|$, and also fixes the number n of radial nodes. Energy levels $\varepsilon_{n,m}$ with $|m|>0$ are twofold degenerate. Instead of this classification, energy eigenstates can be taken as eigenfunctions of the squared angular momentum z component and as symmetric (s) or antisymmetric (a) functions with respect to the parity operation $\vartheta\to-\vartheta$

$$\varphi_{m,n}^{s/a}(r,\vartheta) = \begin{cases} \frac{1}{\sqrt{\pi}}\cos(m\vartheta) & N_{m,n}J_{|m|}\left(\rho_{|m|,n}\frac{r}{R}\right) \quad m = 0,1,2,\ldots, \\ \frac{1}{\sqrt{\pi}}\sin(m\vartheta) & N_{m,n}J_{|m|}\left(\rho_{|m|,n}\frac{r}{R}\right) \quad m = 1,2,3,\ldots. \end{cases} \tag{5}$$

The antisymmetric states $\varphi_{m,n}^{a}$ with a proper normalization, provide a complete set of eigenfunctions of the half-circular billiards. In presence of a static magnetic field $\vec{B}=B\vec{e}_z$, perpendicular to the plane of the circular quantum dot, the kinetic momentum is given by $-i\hbar\vec{\nabla}-q\vec{A}(\vec{r})$, $q=-e$. In the symmetric gauge, $\vec{A}(\vec{r})=(1/2)Br\vec{e}_\vartheta$, the ansatz

$$\varphi_{m,n}(r,\vartheta) = \frac{1}{\sqrt{2\pi C_{m,n}}} e^{im\vartheta} R_{m,n}(r) \tag{6}$$

with $m=0,\pm 1,\pm 2,\ldots$ and

$$R_{m,n}(z) = e^{-z/2} z^{|m|/2} h_{m,n}(z) \tag{7}$$

with $z=r^2/(2l_b^2)$ and the magnetic length $l_b=\sqrt{\hbar/(eB)}$ leads to the confluent hypergeometric differential equation for $h_{m,n}(z)$. Solutions are

$$h_{m,n}(z) = {}_1F_1\left(-\frac{\varepsilon_{m,n}}{\hbar\omega_c} + \frac{1}{2}(m+|m|+1); |m|+1; z\right) \tag{8}$$

with ${}_1F_1$ being a confluent hypergeometric function[18] and the cyclotron frequency $\omega_c=eB/m^*$. Levels are determined by Dirichlet boundary conditions $0=R_{m,n}(R)$, i.e.,

$$0 = {}_1F_1\left(-\frac{\varepsilon_{m,n}}{\hbar\omega_c} + \frac{1}{2}(m+|m|+1); |m|+1; z_0\right) \tag{9}$$

with $z_0=R^2/(2l_b^2)$. We solve Eq. (9) numerically by a path-following method starting from $B=0^+$. The procedure allows to keep track of all levels within a specified energy range. The normalization of the radial wave function $C_{m,n}$ has to be calculated numerically. To illustrate the strength of the magnetic flux density $B=(h/e)n_e z_0/M$ through a quantum dot with M particles, we use a typical electron density $n_e=2.8\times 10^{15}$ m^{-2} per spin orientation.

III. ANDERSON OVERLAP IN RESPONSE TO A LOCALIZED PERTURBATION

A. General method

We address the response of a ballistic mesoscopic electron system to the sudden appearance of a localized perturbation V in terms of the Anderson overlap,[4] i.e., the overlap of many-particle ground states before and after the perturbation is applied.

We label single-particle levels and wave functions of the initial (unperturbed) Hamiltonian H_0 by ε_k and φ_k, respectively, $k=1,\ldots,N$. For our systems of interest, they are introduced in Sec. II. The attractive perturbation V localized at $\vec{r}_c$ is given by a rank-one matrix

$$\langle\varphi_k|V|\varphi_q\rangle = \frac{v_n}{\nu}\varphi_k^*(\vec{r}_c)\varphi_q(\vec{r}_c), \quad k,q = 1,\ldots,N \tag{10}$$

with the asymptotic mean density of states per unit area and spin orientation $\nu=m^*/(2\pi\hbar^2)$. The parameter v_n quantifies the perturbation strength per mean-level spacing and is a measure for the average coupling strength. The quantity $v_n A|\varphi_k(\vec{r}_c)|^2$ can be considered as an effective coupling strength of the state k at the position $\vec{r}_c$ (A denotes the system area). Such a contact type potential is widely employed in the description of the orthogonality catastrophe and x-ray edge problem.[3,7,10,12,19–22]

We refer to the levels and wave functions of the final (perturbed) Hamiltonian H_0+V as λ_κ and ψ_κ, respectively, $\kappa=1,\ldots,N$. The final energy spectrum is determined by the implicit equation[7,23]

$$0 = \frac{1}{v_n} - \frac{1}{\nu}\sum_{k=1}^{N}\frac{\varphi_k^*(\vec{r}_c)\varphi_k(\vec{r}_c)}{\lambda_\kappa - \varepsilon_k}. \tag{11}$$

Final levels are roots of a rational function with N poles at $\varepsilon_1,\ldots,\varepsilon_N$. Except for the lowest final level λ_1 which, for

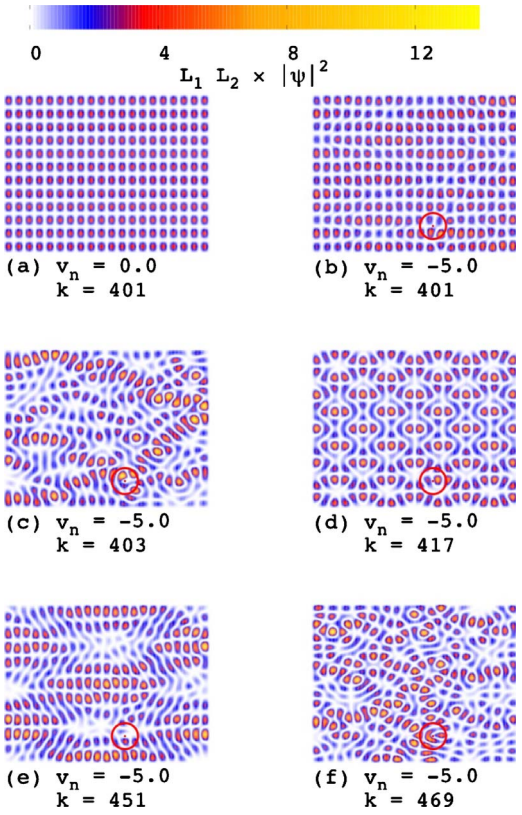

FIG. 1. (Color online) (a) Unperturbed and (b)–(f) perturbed wave functions of the rectangular billiards. The perturbation is placed in the center of the (red) circle. $v_n=-5.0$, $N=2000$, and $\alpha=1.0276$.

sufficiently strong perturbations, drops well below the lowest initial energy level giving rise to the formation of a so-called bound states, final levels are restricted by $\varepsilon_{k-1}<\lambda_k<\varepsilon_k$. Figure 1 illustrates the typical response of wave functions to the appearance of a strong, localized perturbation.

We consider perturbed and unperturbed many-particle ground states $\Psi_0(M)$ and $\Phi_0(M)$, respectively, that are given by Slater determinants composed of the M perturbed and unperturbed single-particle states, respectively, with the lowest energy. The many-particle overlap

$$\Delta = \langle \Psi_0(M) | \Phi_0(M) \rangle \tag{12}$$

is given by the determinant of an $(M\times M)$ matrix (Ref. 19)

$$\Delta = \det(\langle \psi_\kappa | \varphi_k \rangle)_{\kappa,k=1,\ldots,M}. \tag{13}$$

In the case of a rank-one perturbation, cf. Eq. (10), the squared modulus of the overlap of the perturbed and unperturbed many-particle ground states depends, remarkably, only on the unperturbed and perturbed single-particle energy levels[19,23] and can be expressed as

$$|\Delta|^2 = \prod_{i=1}^{M} \prod_{j=M+1}^{N} \frac{(\lambda_i - \varepsilon_j)(\varepsilon_i - \lambda_j)}{(\lambda_i - \lambda_j)(\varepsilon_i - \varepsilon_j)}. \tag{14}$$

We refer to this quantity as the Anderson overlap in the following. We consider systems at half filling $M/N=1/2$. Since the perturbation potential V does not result in a coupling of spins, we neglect the electron spin. Both independent spin components can be treated in the same manner.

B. Anderson overlap in the presence of degeneracies

Equations (11) and (14) do not apply without modifications if the initial energy levels are degenerate. This is the case, e.g., in the circular billiards without external magnetic field: Levels of the circular billiards are either nondegenerate and are related to wave functions with zero angular momentum or are twofold degenerate and can be related to pairs of wave functions with angular momentum of opposite sign, cf. Eq. (3).

We consider a localized perturbation V placed at $(x_c,y_c)=r_c(\cos\vartheta_c,\sin\vartheta_c)$ and choose the coordinate system such that $\vartheta_c=0$. The *antisymmetric* wave functions φ_k^{a} introduced in Eq. (5) vanish at the position of the perturbation and are therefore eigenfunctions in absence *and* presence of the perturbation. Unperturbed degenerate energy levels are split by the perturbation such that the degenerate initial levels persist in presence of the perturbation as nondegenerate levels. The other final energy levels are determined by Eq. (11) summing only over *symmetric* wave functions φ_k^{s}.

Hereafter, we inspect the Anderson overlap of Eq. (12) in presence of degenerate energy levels. It is convenient to introduce fermionic creation and annihilation operators. Particles in initial states with defined angular momentum φ_k [Eq. (3)] are created by $c_k^\dagger$, particles in initial states with an even (s) or odd (a) parity $\varphi_k^{\mathrm{s/a}}$ [Eq. (5)] are created by $c_k^{\mathrm{s/a}\dagger}$ and particles in final states ψ_κ are created by $d_\kappa^\dagger$.

In the following, we fix the number of electrons M such that, in the ground state

$$|\Phi_0(M)\rangle = c_M^\dagger c_{M-1}^\dagger c_{M-2}^\dagger \ldots c_1^\dagger |0\rangle, \tag{15}$$

the highest initial level is twofold degenerate and fully occupied. In this case, the Anderson overlap $|\langle \Psi_0(M)|\Phi_0(M)\rangle|^2$ is determined by Eq. (14) taking only initial and final levels into account that belong to symmetric wave functions.

We obtain the Anderson overlap of a system with $M-1$ electrons and the initial state

$$|\Phi_0(M-1)\rangle = c_{M-1}^\dagger c_{M-2}^\dagger c_{M-3}^\dagger \ldots c_1^\dagger |0\rangle \tag{16}$$

by the following consideration: We use the relation between initial creation operators

$$c_M^{\mathrm{a}\dagger} = \frac{1}{i\sqrt{2}}(c_M^\dagger - c_{M-1}^\dagger), \tag{17}$$

and recapitulate that initial antisymmetric states solve the final Schrödinger equation, too,

$$d_M^\dagger = c_M^{\mathrm{a}\dagger}. \tag{18}$$

The Anderson overlaps of the $M-1$ and M-electron systems are related by

$$
\begin{aligned}
&|\langle\Psi_0(M-1)|\Phi_0(M-1)\rangle|^2 \\
&\quad = |\langle 0|d_1 \ldots d_{M-1} c_{M-1}^\dagger \ldots c_1^\dagger|0\rangle|^2 \\
&\quad = |\langle 0|d_1 \ldots d_{M-1} d_M c_M^{a\dagger} c_{M-1}^\dagger \ldots c_1^\dagger|0\rangle|^2 \\
&\quad = \frac{1}{2}|\langle 0|d_1 \ldots d_{M-1} d_M (c_M^\dagger - c_{M-1}^\dagger) c_{M-1}^\dagger \ldots c_1^\dagger|0\rangle|^2 \\
&\quad = \frac{1}{2}|\langle\Psi_0(M)|\Phi_0(M)\rangle|^2. \qquad (19)
\end{aligned}
$$

We note that the initial many-particle ground state of $M-1$ electrons is not unique due to the two dimensionality of the eigenspace of the degenerate level. Therefore we consider an average over two independent initial many-particle ground states of $M-1$ electrons. Instead of

$$|\Phi_0(M-1)\rangle = c_{M-1}^\dagger c_{M-2}^\dagger c_{M-3}^\dagger \ldots c_1^\dagger|0\rangle, \qquad (20)$$

one may consider

$$|\Phi_0^{\mathrm{a}}(M-1)\rangle = c_M^{\mathrm{a}\dagger} c_{M-2}^\dagger c_{M-3}^\dagger \ldots c_1^\dagger|0\rangle \qquad (21)$$

or

$$|\Phi_0^{\mathrm{s}}(M-1)\rangle = c_{M-1}^{s\dagger} c_{M-2}^\dagger c_{M-3}^\dagger \ldots c_1^\dagger|0\rangle. \qquad (22)$$

Writing the Anderson overlap $|\Delta|^2 = \mathrm{tr}(P_{\Psi_0} P_{\Phi_0})$ as an expectation value of the projection operator $P_{\Psi_0} = |\Psi_0\rangle\langle\Psi_0|$ and substituting the pure state $P_{\Phi_0} = |\Phi_0\rangle\langle\Phi_0|$ by the mixed state

$$\rho(M-1) = \frac{1}{2}(P_{\Phi_0^{\mathrm{a}}(M-1)} + P_{\Phi_0^{\mathrm{s}}(M-1)}), \qquad (23)$$

we get the counterpart of Eq. (19)

$$
\begin{aligned}
\mathrm{tr}[P_{\Psi_0(M-1)}\rho(M-1)] &= \frac{1}{2}\mathrm{tr}(P_{\Psi_0(M-1)} P_{\Phi_0^{\mathrm{s}}(M-1)}) \\
&= \frac{1}{2}\mathrm{tr}(P_{\Psi_0(M)} P_{\Phi_0(M)}). \qquad (24)
\end{aligned}
$$

According to Eq. (19), which applies to specific initial many-particle states [Eq. (16)], and according to Eq. (24), which holds for a certain average [Eq. (23)], the Anderson overlap of a system with $M-1$ electrons, where the highest occupied energy level is twofold degenerate but incompletely filled, is reduced by a factor of 1/2 compared to the Anderson overlap of a system with an additional electron.

A similar approach can be formulated for a system with an g-fold degenerate initial level where $g-1$ energy eigenfunctions are not affected by the localized perturbation. It is outlined in the Appendix A. As a result, the factor 1/2 in Eq. (24) has to be substituted by $1/g$. The behavior was confirmed in a numerical study of AOC in quantum dots with parabolic confinement potential.[11]

C. Bulklike model and reference overlap Δ_b

For later comparison to the mesoscopic case, we introduce the so-called bulklike model,[3] defined by (i) equidistant energy levels and (ii) uniform wave-function intensities, $|\varphi_k|^2 = 1/A$, with A being the area of the system. We refer to the Anderson overlap of this bulklike (reference) system as $|\Delta_b|^2$. It is well known that $|\Delta_b|^2$ follows a power law in the number of particles in the system and tends to zero in the thermodynamic limit, which is known as the Anderson orthogonality catastrophe.[4]

Ohtaka and Tanabe give the power law in the form[19]

$$|\Delta_b|^2 = C_0 N_{\mathrm{eff}}^{-(\delta_0(\varepsilon_F)/\pi)^2} \qquad (25)$$

with the effective number of particles N_{eff} in the band that is given by band width times density of states at the Fermi level and some constant C_0. Note that the exponent is determined by the phase shift $\delta_0(\varepsilon_F)$ at the Fermi energy that is induced by the localized perturbing potential.

Below we will use $|\Delta_b|^2$ as obtained from Eq. (14) to scale (normalize) the overlaps of individual mesoscopic systems in order to remove their dependence on the number of particles in the system.

IV. RESULTS

In this section, we discuss probability distributions of Anderson overlaps in ballistic mesoscopic systems. Initially, we consider rectangular and half-circular billiards as integrable examples. We compare our results to both the bulklike case and a generic chaotic system. In the second section, we study the circular billiards, again in comparison to the chaotic case, and focus on the impact of level degeneracies on the overlap distribution.

A. AOC and overlap distributions in rectangular and half-circular vs chaotic quantum billiards

We start our studies with the two-dimensional rectangular quantum dot with hard walls.[24] Mesoscopic fluctuations become evident as the number of electrons in the system (corresponding to a size variation of experimental samples) is varied from $M=50-1000$, cf. Fig. 2. The position of the localized perturbation strongly influences the effective coupling strength of wave functions, cf. Eqs. (10) and (11). We average out this spatial dependence by considering 5000 random positions of the perturbation. The residual sensitivity of the overlap on the particle number is shown by the open symbols in Fig. 2 for both a weak and a strong perturbation. The still significant fluctuations indicate that the distribution of electron levels near the Fermi level plays a special role.[3,10] Averaging furthermore over a small range of particle numbers ΔM, i.e., $M = \langle M\rangle - \Delta M, \ldots, \langle M\rangle + \Delta M$, results in a smooth dependence of the mean overlap on the mean particle number. We will employ such an averaging procedure throughout the paper.

Evidently, AOC is incomplete and the overlap is larger than zero for this finite number of particles well below the thermodynamic limit. Comparing the average mesoscopic Anderson overlap to the bulklike reference value, denoted by filled symbols and solid lines in Fig. 2, respectively, makes clear that both values coincide for strong perturbations (lower curve). For weak perturbations (upper curve), however, the effect of the orthogonality catastrophe is more pronounced in the rectangular mesoscopic system.

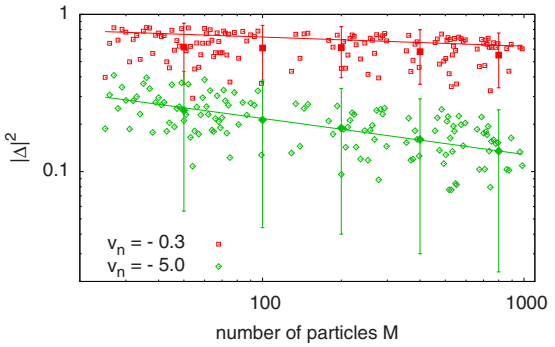

FIG. 2. (Color online) Dependence of the Anderson overlap $|\Delta|^2$ on the particle number M for a weak perturbation, $v_n=-0.3$ (red squares) and a strong perturbation, $v_n=-5.0$ (green diamonds) in the case of the rectangular dot as log-log plot. Solid lines indicate the power law for the Anderson overlap in the corresponding bulklike system. Mesoscopic fluctuations (open symbols) are clearly visible although each value denoted by an open symbol is obtained by averaging over at least 5000 positions of the localized perturbation for every particle number. The filled symbols (with vertical error bars denoting the standard deviation) are obtained when additionally averaging the Anderson overlap over a certain range of particle numbers ΔM (corresponding to experimental systems of slightly varying size), $\Delta M=10$ for the lowest $\langle M\rangle=50$ and $\Delta M=30$ otherwise. Whereas these values fit the power law of the bulklike model in the case of strong perturbations, a clear deviation occurs for weak perturbations. Here, AOC is on average stronger in the mesoscopic system.

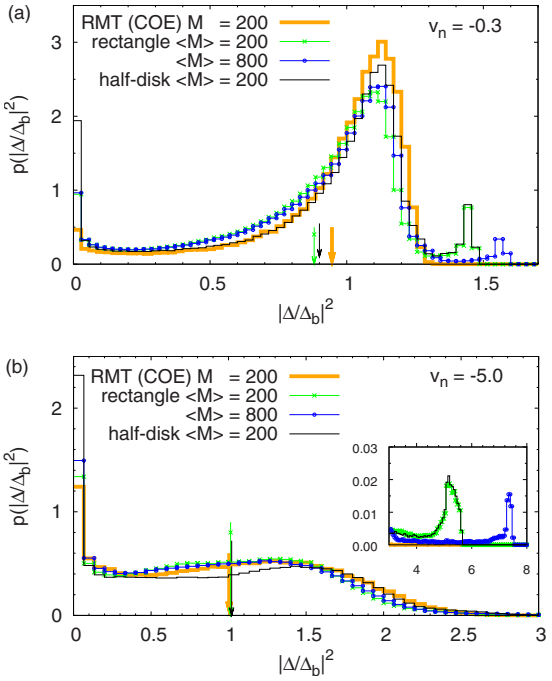

FIG. 3. (Color online) Probability distribution of scaled Anderson overlaps $p(|\Delta/\Delta_b|^2)$ for a rectangular quantum dot in the Golden ratio and a half-circular dot. Particle numbers $\langle M\rangle=200$ and 800 are considered for a weak perturbation $v_n=-0.3$ in panels (a) as well as for a strong perturbation $v_n=-5.0$ in panel (b); the inset shows the tails with side peaks representing an M-dependent boundary effect. Apart form that, the distributions are independent of the particle number. At least 10 000 positions of the perturbation are sampled, $\Delta M=45$. The chaotic case (RMT, COE) is shown for comparison. The differences between the integrable and the chaotic system are small but characteristic and result in smaller average overlaps, shown by arrows for $\langle M\rangle=200$, in the integrable systems than in the chaotic system for weaker perturbation strengths.

In order to remove the overall M dependence of the Anderson overlap so that a comparison of mesoscopic systems with different electron numbers M becomes meaningful, we scale the overlap $|\Delta|^2$ of the mesoscopic system by the overlap $|\Delta_b|^2$ of the corresponding bulklike system. Distributions of scaled Anderson overlaps $p(|\Delta/\Delta_b|^2)$ in the rectangular quantum dot are shown in Figs. 3(a) and 3(b) for a weak and a strong perturbation, respectively. Except for boundary effects, that we discuss below, they are, for one and the same system type, practically independent of the mean particle number $\langle M\rangle$. All distributions exhibit a maximum near $|\Delta/\Delta_b|^2\simeq 1$, a peak at zero with its size depending on the perturbation strength and the confinement geometry, and smaller peaks at large scaled overlaps that depend on the particle number $\langle M\rangle$ and are a result of boundary effects. We do not find a pronounced dependence of the scaled overlap distribution on the aspect ratio of the rectangle $L_1/L_2=\sqrt{\alpha}$. Using, e.g., $\alpha=\sqrt{2}$ instead of the Golden ratio $\alpha=(1+\sqrt{5})/2$ employed in Fig. 3, yields very similar distributions. Only for ratios close to an integer, e.g., 1.000029 or 4.0000033, we observed clear deviations due to the presence of (nearly) degenerate levels.

The small side peaks beyond the main maximum arise from events where the perturbation is placed near the system boundary. Recalling that all single-particle wave functions tend to zero near the hard wall, clarifies that the closer the perturbation is placed to the boundary, the smaller is the effective coupling of single-particle wave functions and the larger is the Anderson overlap constrained by the upper limit one. The scaling by the overlap of the bulklike system produces the side peaks at values $\approx 1/|\Delta_b|^2$. Once such events are excluded from the averaging, those peaks disappear. Increasing the mean number of electrons M, reduces the impact of this boundary effect, which can be seen in Figs. 3(a) and 3(b).

Besides the data for the rectangular billiards, Fig. 3 shows the overlap distributions of half-circular billiards and of chaotic mesoscopic systems modeled by random-matrix theory (RMT) (circular orthogonal ensemble, COE), which was previously reported.[3,10] The presence of system boundaries is not included in the random-matrix description of chaotic systems; this has to be taken into account when comparing the generic chaotic case and the integrable billiard systems.

Apart from the side peaks, the overlap distributions of both integrable billiards systems and the generic chaotic system are rather similar with small deviations: (i) The probability density for vanishing Anderson overlaps is the lowest in the chaotic system. The value in the half circle is much higher than that in the rectangle. (ii) The distribution for the half disk falls below that of the rectangle before the main maximum, and above it beyond. This holds for both a weak and a strong perturbation. Below the main maximum, the chaotic distribution is close to the distribution of the half

disk, if the perturbation is weak, and close to the distribution of the rectangle, if the perturbation is strong. The chaotic model shows the highest probability density above the main maximum in the tail of the distribution for the weak perturbation.

Mean values of the scaled Anderson overlap in the rectangle and half disk fall below the mean value of the chaotic system which are smaller than one for a weak perturbation, cf. Figs. 2 and 3(a). If the perturbation is strong, all mean values are close to one. A certain understanding for this behavior is provided using the so-called range-one approximation[3,10] where the same ordering of the overlaps is seen.[25] A detailed study of average Anderson overlap values is provided in Appendix B.

Placing a point scatter in a rectangular quantum billiards induces so-called wave chaos,[26–28] whereas a chaotic system is expected to remain chaotic. This statement might suggest a stronger effect of a localized perturbation, measured in terms of the Anderson overlap, in the rectangular billiards than in a chaotic system. Our data show, however, that this difference is very small and only relevant for small and modest perturbation strengths.

The differences in the distributions at vanishing Anderson overlap can be understood as follows. For the chaotic case[10] (COE), it was stated that the distribution of scaled overlaps exhibits a peak at $|\Delta/\Delta_b|^2=0$ that is related to the divergence of the Porter-Thomas distribution for the wave-function intensities I at $I=0$. The argument applies here as well. The probability of finding a small intensity $I\in[0,\delta]$, $0<\delta\ll 1$ is highest in the half disk followed by the rectangular billiards and the chaotic system.[29] The strong decrease in the Anderson overlap due to fluctuating and in particular small wave intensities can be qualitatively understood by the following argument: Let us assume an initial ground state of M electrons and the perturbation placed at $\vec{r}_c$. Let us further assume that the single-particle wave function at the Fermi level vanishes, $\varphi_M(\vec{r}_c)=0$, thus, φ_M remains an eigenstate with energy ε_M for every perturbation strength. In the calculation of the perturbed energy levels Eq. (11), it simply drops out of the sum. Now, we reduce the parameter v_n continuously starting at $v_n=0$. The perturbed energy levels λ_κ depend on v_n in general, cf. Eq. (11), and it is possible that the perturbed level $\lambda_{M+1}(v_n)$, originating from the unperturbed level ε_{M+1}, crosses the level $\lambda_M=\varepsilon_M$ at some v_n^*. At the crossing v_n^*, we have to resort the levels (and states) such that $\lambda_M<\lambda_{M+1}$. Beyond the crossing $v_n<v_n^*$, we obtain

$$\langle\psi_k|\varphi_M\rangle=0 \quad \text{for} \quad k=1,\ldots,M. \tag{26}$$

This means that one column of the matrix, whose determinant gives the Anderson overlap Eq. (12), contains as entries only zeros, thus

$$\langle\Psi_0(M)|\Phi_0(M)\rangle=0. \tag{27}$$

If we now replace the assumption $\varphi_M(\vec{r}_c)=0$ by $|\varphi_M(\vec{r}_c)|^2\ll 1/A$, we get an avoided level crossing instead of the level crossing, but the many-particle overlap still drops considerably. An example is pictured in Fig. 4.

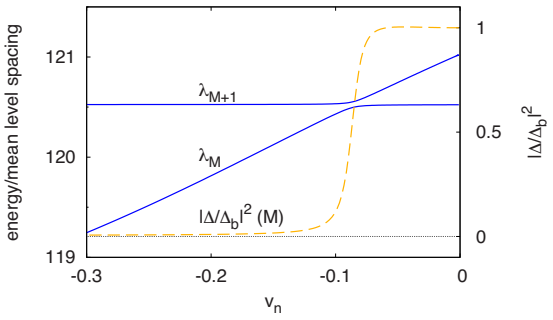

FIG. 4. (Color online) As v_n is reduced from $v_n=0$, an avoided level crossing appears induced by a small intensity $|\varphi_M(\vec{r}_c)|^2$. The many-particle overlap drops strongly since the Fermi level is involved in the avoided level crossing. Shown is an example of the half-circular billiards.

B. AOC in circular quantum billiards: Impact of level degeneracies

We now investigate circular ballistic quantum dots as a third integrable system. Our focus will be on the impact of level degeneracies on the many-particle overlap distributions. For comparison, we also consider the circular dot in the presence of a magnetic field where level degeneracies are lifted.

Figure 5 shows distributions of scaled Anderson overlaps in circular billiards exemplarily in the case of a weak perturbation. Again, they are similar for all considered particle numbers $\langle M\rangle=100$, 200, and 800. The new feature of the distribution is a central maximum. Its position is at about one half of the Anderson overlap value of the maximum near $|\Delta/\Delta_b|^2\simeq 1$ (that is familiar from all previously considered cases). The factor of 1/2 and the double-peak structure are a direct consequence of the presence of twofold degenerate levels and can be understood from Eq. (19). This equation states that the overlap of the system with $M-1$ particles, corresponding to a single occupation of a twofold degenerate initial level, is a factor of two smaller than the overlap of the system with M particles, i.e., a fully occupied degenerate initial level. In other words, the distribution in the presence of twofold degenerate levels can be approximately thought of as obtained by superposing that obtained with fully occupied levels plus a copy of the latter distribution stretched by a factor of 1/2.

A more qualitative argument can be given in terms of the available phase space: A single electron on a twofold degenerate (or nearly degenerate) level can, in the course of the sudden perturbation, "rechoose" on which of the two levels it wants to be. This amounts to a factor of 1/2 in the corresponding Anderson overlap. Generalization to g-fold degenerate levels is straightforward and results in a factor $1/g$. Applying the picture of a two-level system, we get the following reasoning: A singly occupied initially degenerate level is split by a sudden perturbation. Without additional knowledge about the initial state, we expect with a probability of 1/2 to find the particle in the state with the lower energy finally.

Level degeneracies can be removed by breaking the responsible system symmetries. In the case of the circular bil-

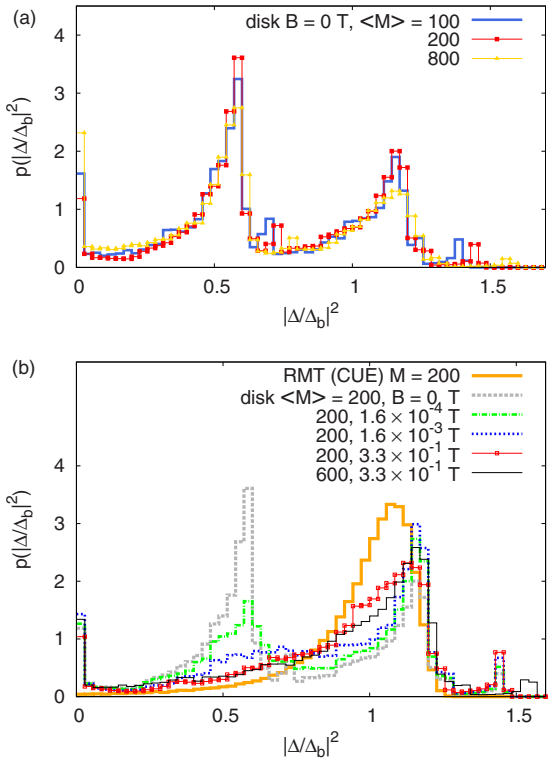

FIG. 5. (Color online) Distributions of scaled overlaps $p(|\Delta/\Delta_b|^2)$ in circular billiards in the case of a weak perturbation $v_n=-0.3$. (a) Without magnetic field, twofold degenerate levels result in the presence of two pronounced maxima in addition to the peak at vanishing overlap. The central maximum is a distinct difference to the behavior of systems without level degeneracies. The average overlap is therefore considerably reduced compared to the billiards without level degeneracies (Fig. 3). The positions of the maxima are related by a factor of 1/2 corresponding to the inverse of the degree of degeneracy. (b) Turning on an external magnetic field splits degenerate levels and results, eventually, in the disappearance of the central peak. At $B=3.3\times10^{-1}$ T, overlap distributions for different particle numbers coincide, shown for $\langle M\rangle=200$ and 600, moreover, we find very similar distributions at $B=3.3\times10^{-2}$ T which indicates a saturation. We sample 10 000 positions of the perturbation and a range of particle numbers $\Delta M=30$. Note that Anderson overlaps of the circular billiards in a magnetic field are differently distributed than those of the corresponding generic chaotic systems with broken time-reversal symmetry described by RMT (CUE).

liards one can break the time reversal symmetry by applying a magnetic field, or the rotational symmetry by considering, for example, the half-circular billiards which is described in the previous section.

The presence of a magnetic field separates levels by $|\varepsilon_{m,n}-\varepsilon_{-m,n}|=\hbar\omega_c m$, with $\omega_c=eB/m^*$ the cyclotron frequency. We address the range of modest magnetic fields where Landau levels are not yet formed. Figure 5(b) shows distributions of scaled overlaps for systems in a finite magnetic field.[30] The degeneracy-caused double-peak structure in the distributions disappears gradually when the magnetic field is increased.

Remnants of the degeneracy caused central peak are still clearly visible at $B=1.6\times10^{-3}$ T $(1.6\times10^{-4}$ T) in Fig. 5(b). We estimate the corresponding level splitting at the Fermi energy compared to the mean-level spacing d for $M=170,\ldots,230$, with the relevant azimuthal quantum numbers m, $1\le m\le24$, $\langle m\rangle\approx10$, to be $|\varepsilon_{m,n}-\varepsilon_{-m,n}|/d=m\times0.028(0.0028)$, i.e., on the order of one tenth of the mean-level spacing. Even for this rather big splitting, the overlap distribution is still affected by the former level degeneracies.

The comparison of the overlap distribution at $B=3.3\times10^{-1}$ T to the corresponding generic chaotic systems described by RMT (circular unitary ensemble, CUE) in Fig. 5(b) [thick solid (yellow) line] reveals a more pronounced difference in the distribution than observed for rectangular and half-circular quantum dots in the presence of time-reversal symmetry. For the chaotic system, the distribution is more narrow than in the circular system. In addition, the probability of having vanishing overlap was found to be very small in chaotic systems with magnetic field,[3,10] but remains high in the regular case with values similar to those found without magnetic field.

V. SUMMARY AND CONCLUSION

We considered Anderson orthogonality catastrophe (AOC) in mesoscopic ballistic systems. In contrast to the metallic case, the finite particle numbers yield finite Anderson overlaps with a broad distribution. On average, the dependence of the overlap on the particle number reproduces the Anderson power law of a bulklike model for strong perturbations and falls slightly below the power law for weak perturbations. Distributions of overlaps scaled by the overlaps of a bulklike system are independent of the particle number except for small side peaks that reflect boundary effects that were not considered in the previously studied chaotic case.[10]

Comparing scaled overlap distributions for a rectangular and half-circular billiards, we find only a weak dependence on the geometrical confinement. Moreover, the scaled overlap distributions of the two regular systems are rather similar to distributions of chaotic systems described by random-matrix theory. Different statistical properties of energy levels and wave functions, typically considered as characteristics of integrable and chaotic quantum systems, result only to a minor degree in differences in the distributions of Anderson overlaps. A slightly larger weight on smaller and vanishing overlaps is found for the integrable billiards systems in the case of a weak perturbation. The different portion of vanishing overlaps originates in the different, system-dependent intensity distributions of the wave functions. Altogether, we find, that, in general, *the geometry of the confinement of a ballistic quantum dot does not affect the distribution of Anderson overlaps remarkably*. However, this changes drastically in the presence of level degeneracies, such as in the circular quantum billiards. The twofold level degeneracies of the circular billiards lead to an additional maximum in the probability distribution of the Anderson overlap. The positions of the additional and of the main peak are related by a factor of about 1/2 (or1/degeneracy). This results in a considerable reduction in the average Anderson overlap, i.e., *level degeneracies imply a strong enhancement of the or-*

thogonality catastrophe. Besides the circular quantum dot studied here, level degeneracies occur also, e.g., in parabolic quantum dots and carbon nanotubes.

We described analytically that a system with an incompletely filled twofold degenerate level possesses half the Anderson overlap of the system with an additional electron. The decrease by the factor 1/2 is caused by a nontrivial kernel of the rank-one perturbation restricted to the two-dimensional eigenspace of a degenerate level, more physically, it reflects a phase-space factor. The generalization to the g-fold degenerate case is straight forward, cf. Appendix A.

Lifting the level degeneracies of the circular billiards by applying an external magnetic field, gradually dissolves the degeneracy peak in the overlap distribution. Its trace can be followed up to a level splitting at the Fermi energy on the order of one tenth of the mean-level spacing. Provided that the degeneracy peak is resolved in a moderate magnetic field, the overlap distribution differs from that obtained for a chaotic system described by random-matrix theory (CUE), i.e., in the presence of a magnetic field (broken time-reversal symmetry) we find a stronger geometry dependence of the Anderson overlap.

ACKNOWLEDGMENTS

We thank Swarnali Bandopadhyay, Harold Baranger, Eduardo Mucciolo, Rainer Bedrich, Klaus Richter, Jens Siewert, Steven Tomsovic, and Denis Ullmo for discussions and the German Research Foundation (DFG) for support in the Emmy-Noether Programme. M.H. thanks the Robert-Bosch-Foundation for support in the Fast Track Program.

APPENDIX A: MANY-PARTICLE OVERLAP AND G-FOLD DEGENERACIES

We consider the application of a rank one perturbation V of Eq. (10) to a noninteracting electron system H_0 with an g-fold degenerate single-particle level. V, restricted to the g-dimensional eigenspace, possesses an $g-1$ dimensional kernel. As a consequence, on an average, the squared modulus of the overlap of the unperturbed and perturbed many-particle ground states of a system with a singly occupied degenerate initial level is reduced by $1/g$ compared to the Anderson overlap of the system with all g eigenstates of the degenerate level being occupied.

To show this, we consider an orthonormal basis $\varphi_{k,j}$ and levels ε_k that solve

$$H_0\varphi_{k,j} = \varepsilon_k\varphi_{k,j}. \tag{A1}$$

k enumerates levels and $j=1,\ldots,g_k$ counts the g_k degeneracies of the each level. The number of states N (cutoff) is fixed. We add the perturbation V of Eq. (10) that acts at $\vec{r}_c$ and consider the equation

$$(H_0+V)\psi_{k,j} = \lambda_{k,j}\psi_{k,j}. \tag{A2}$$

We assume $\varphi_{k,j}(\vec{r}_c)\neq 0$. We construct a basis $\chi_{k,j}$ in the g_k-dimensional eigenspace of ε_k:

$$\chi_{k,1} = \frac{1}{\sqrt{\sum_{j=1}^{g_k}|\varphi_{k,j}(\vec{r}_c)|^2}}\sum_{j=1}^{g_k}\varphi_{k,j}^*(\vec{r}_c)\varphi_{k,j}, \tag{A3}$$

$$\tilde{\chi}_{k,j} = \frac{1}{\sqrt{|\varphi_{k,j}(\vec{r}_c)|^2+|\varphi_{k,1}(\vec{r}_c)|^2}}\times(\varphi_{k,j}(\vec{r}_c)\varphi_{k,1}-\varphi_{k,1}(\vec{r}_c)\varphi_{k,j}),$$

$$j=2,\ldots,g_k. \tag{A4}$$

It holds for $j=2,\ldots,g_k$

$$\langle\chi_{k,1}|\tilde{\chi}_{k,j}\rangle = 0, \tag{A5}$$

$$(H_0+V)\tilde{\chi}_{k,j} = H_0\tilde{\chi}_{k,j}, \tag{A6}$$

$$=\varepsilon_k\tilde{\chi}_{k,j}. \tag{A7}$$

One may orthogonalize the g_k-1 linearly independent $\tilde{\chi}_{k,j}$ by a Gram-Schmidt process, normalize and label the result $\chi_{k,j}$ and identify

$$\psi_{k,j} = \chi_{k,j} \quad \text{for} \quad j=2,\ldots,g_k. \tag{A8}$$

If V is attractive then $\lambda_{k,1}<\lambda_{k,j}=\varepsilon_k$, $j=2,\ldots,g_k$.

We introduce fermionic creation operators: Particles in states $\varphi_{k,j}$ are created by $c_{k,j}^\dagger$, particles in states $\chi_{k,j}$ are created by $a_{k,j}^\dagger$ and particles in states $\psi_{k,j}$ are created by $d_{k,j}^\dagger$. $c_{k,j}^\dagger$ and $a_{k,j}^\dagger$ are related by unitary $(g_k\times g_k)$-matrices $\mathcal{U}^k=(u_{jj'}^k)_{j,j'=1,\ldots,g_k}$

$$c_{k,j}^\dagger = \sum_{j'=1}^{g_k}u_{jj'}^k a_{k,j'}^\dagger, \tag{A9}$$

$$u_{jj'}^k = \langle\chi_{k,j'}|\varphi_{k,j}\rangle. \tag{A10}$$

We define the initial and final ground states of $M=\sum_{k=1}^{k_M}g_k$ particles

$$|\Phi_0(M)\rangle = c_{k_M,g_{k_M}}^\dagger\ldots c_{1,1}^\dagger|0\rangle, \tag{A11}$$

$$|\Psi_0(M)\rangle = d_{k_M,g_{k_M}}^\dagger\ldots d_{1,1}^\dagger|0\rangle. \tag{A12}$$

The initial ground state with $M+1$ particles is ambiguous, the final state with $M+1$ particles is unique

$$|\Phi_0^j(M+1)\rangle = c_{k^*,j}^\dagger|\Phi_0(M)\rangle, \tag{A13}$$

$$|\Psi_0(M+1)\rangle = d_{k^*,1}^\dagger|\Psi_0(M)\rangle \tag{A14}$$

with $k^*=k_M+1$. The many-particle overlap of ground states with $M+1$ particles assuming the initial state $\varphi_{k^*,j}$ being occupied yields

$$
\begin{aligned}
&|\langle\Psi_0(M+1)|\Phi_0^j(M+1)\rangle|^2 \\
&\quad = |\langle\Psi_0(M)|d_{k^*,1}c^\dagger_{k^*,j}|\Phi_0(M)\rangle|^2 \\
&\quad = |\langle\Psi_0(M)|d_{k^*,1}d_{k^*,2}\ldots d_{k^*,g_{k^*}}a^\dagger_{k^*,g_{k^*}}\ldots a^\dagger_{k^*,2}c^\dagger_{k^*,j}|\Phi_0(M)\rangle|^2 \\
&\quad = |u^{k^*}_{j1}|^2 \\
&\quad \times|\langle\Psi_0(M)|d_{k^*,1}\ldots d_{k^*,g_{k^*}}a^\dagger_{k^*,g_{k^*}}\ldots a^\dagger_{k^*,2}a^\dagger_{k^*,1}|\Phi_0(M)\rangle|^2 \\
&\quad = |u^{k^*}_{j1}|^2|\langle\Psi_0(M)|d_{k^*,1}\ldots d_{k^*,g_{k^*}}c^\dagger_{k^*,g_{k^*}}\ldots c^\dagger_{k^*,2}c^\dagger_{k^*,1}|\Phi_0(M)\rangle|^2 \\
&\quad = |u^{k^*}_{j1}|^2|\langle\Psi_0(M+g_{k^*})|\Phi_0(M+g_{k^*})\rangle|^2 \qquad \text{(A15)}
\end{aligned}
$$

using Eqs. (A8) and (A9). Averaging by means of the density matrix

$$\rho(M+1)=\frac{1}{g_{k^*}}\sum_{j=1}^{g_{k^*}}P_{\Phi_0^j(M+1)} \qquad \text{(A16)}$$

using $P_{\Phi_0^j(M+1)}=|\Phi_0^j(M+1)\rangle\langle\Phi_0^j(M+1)|$ yields

$$\mathrm{tr}[P_{\Psi_0(M+1)}\rho(M+1)]=\frac{1}{g_{k^*}}\mathrm{tr}[P_{\Psi_0(M+g_{k^*})}P_{\Phi_0(M+g_{k^*})}]. \qquad \text{(A17)}$$

APPENDIX B: MEAN-SCALED ANDERSON OVERLAPS

Whereas we focused on overlap distributions in the body of the paper, we add here a detailed discussion of mean-scaled Anderson overlaps $\langle|\Delta/\Delta_b|^2\rangle$ for the rectangular and half-circular billiards as well as for the COE, see Fig. 6. Data are obtained by ensemble averaging as described in Sec. IV. We study the mean values as a function of the perturbation strength that we parameterize by the phase shift δ_0 of the bulklike system at the Fermi level, $\tan\delta_0=-\pi v_n$ for $M/N=1/2$.[10,23] We find, for both billiard systems, a nonmonotonous dependence of $\langle|\Delta/\Delta_b|^2\rangle$ on δ_0. $\langle|\Delta/\Delta_b|^2\rangle$ falls below 1 except for very strong perturbations and exhibits a local minimum at about $\delta_0=\pi/4$ $(v_n\approx-0.3)$. The same qualitative behavior is found for the COE, although the averaged Anderson overlap of this chaotic system is generally closer to the bulklike reference value, cf. Fig. 6. We thus observe, on average, an enhancement of the AOC in the integrable billiards, even in the absence of level degeneracies.

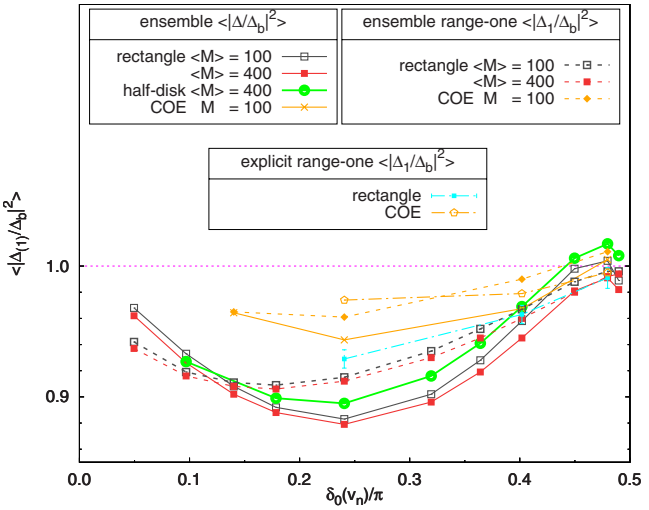

FIG. 6. (Color online) Mean-scaled Anderson overlap $\langle|\Delta/\Delta_b|^2\rangle$ in dependence on the phase shift δ_0 at the Fermi level. Shown are data for the rectangular billiards, half-circular billiards, and a generic chaotic system (COE). We sample at least 12 000 positions of the perturbation in the billiards, $\Delta M=45$. The mean-scaled Anderson overlap in range-one approximation $\langle|\Delta_1/\Delta_b|^2\rangle$ is also shown. Within this approximation, $\langle|\Delta_1/\Delta_b|^2\rangle$ can be determined by means of an explicit integral equation (points "explicit"), see text for details. Error bars indicate numerical integration errors.

In Fig. 6, we also compare these results to mean-scaled Anderson overlaps $\langle|\Delta_1/\Delta_b|^2\rangle$ obtained in the so-called range-one approximation, introduced in Refs. 3 and 10. This approximation allows one to derive an explicit equation for $p(|\Delta/\Delta_b|^2)$ in dependence on the level spacing distribution and intensity distribution of wave functions; in Fig. 6 we refer to the latter approach as explicit method in contrast to the ensemble averaging. Regarding the explicit method, we describe the rectangular billiards by means of the level-spacing distribution $p_s(s)=\exp(-s)$ (Poisson) and a closed expression for the intensity distribution.[29] Correlations at the system boundary are neglected here. In the case of small and moderate perturbation strengths, the range-one approximation reproduces the relative ordering of mean-scaled Anderson overlaps of the rectangle, the COE, and the bulklike system.

[1] D. Goldhaber-Gordon, H. Shtrikman, D. Mahalu, D. Abusch-Magder, U. Meirav, and M. A. Kastner, Nature (London) **391**, 156 (1998).
[2] S. M. Cronenwett, T. H. Oosterkamp, and L. P. Kouwenhoven, Science **281**, 540 (1998).
[3] M. Hentschel, D. Ullmo, and H. U. Baranger, Phys. Rev. Lett. **93**, 176807 (2004).
[4] P. W. Anderson, Phys. Rev. Lett. **18**, 1049 (1967).
[5] G. D. Mahan, *Many Particle Physics* (Kluwer Academic, Plenum, New York, 2000).
[6] P. Nozières and C. T. de Dominicis, Phys. Rev. **178**, 1097 (1969).
[7] K. Ohtaka and Y. Tanabe, Rev. Mod. Phys. **62**, 929 (1990).
[8] R. O. Vallejos, C. H. Lewenkopf, and Y. Gefen, Phys. Rev. B **65**, 085309 (2002).
[9] Y. Gefen, R. Berkovits, I. V. Lerner, and B. L. Altshuler, Phys. Rev. B **65**, 081106(R) (2002).
[10] M. Hentschel, D. Ullmo, and H. U. Baranger, Phys. Rev. B **72**,

035310 (2005).
[11] S. Bandopadhyay and M. Hentschel (unpublished).
[12] M. Hentschel and F. Guinea, Phys. Rev. B **76**, 115407 (2007).
[13] M. Hentschel, G. Röder, and D. Ullmo, Prog. Theor. Phys. **166**, 143 (2007).
[14] A. M. Chang, H. U. Baranger, L. N. Pfeiffer, and K. W. West, Phys. Rev. Lett. **73**, 2111 (1994).
[15] C. M. Marcus, A. J. Rimberg, R. M. Westervelt, P. F. Hopkins, and A. C. Gossard, Phys. Rev. Lett. **69**, 506 (1992).
[16] F. Geerinckx, F. M. Peeters, and J. T. Devreese, J. Appl. Phys. **68**, 3435 (1990).
[17] R. Liboff, *Introductory Quantum Mechanics* (Addison-Wesley, Reading, MA, 2003).
[18] M. Abramowitz and I. A. Stegun, *Handbook of Mathematical Functions with Formulas, Graphs, and Mathematical Tables* (Dover, New York, 1964).
[19] Y. Tanabe and K. Ohtaka, Phys. Rev. B **32**, 2036 (1985).
[20] L. A. Feldkamp and L. C. Davis, Phys. Rev. B **22**, 4994 (1980).
[21] K. D. Schotte and U. Schotte, Phys. Rev. **182**, 479 (1969).
[22] M. Hentschel, D. Ullmo, and H. U. Baranger, Phys. Rev. B **76**, 245419 (2007).
[23] I. L. Aleiner and K. A. Matveev, Phys. Rev. Lett. **80**, 814 (1998).
[24] Numerical calculations for the rectangular as well as the half-circular billiards are performed by means of an unfolded energy spectrum to ensure a uniform mean-level spacing as in the chaotic systems described by RMT. The unfolding has, however, only a very small effect on the overlap distributions. F. Haake, *Quantum Signature of Chaos* (Springer, New York, 2001); M. C. Gutzwiller, *Chaos in Classical and Quantum Mechanics* (Springer, New York, 1990).
[25] G. Röder, doctoral dissertation in preparation.
[26] P. Šeba and K. Życzkowski, Phys. Rev. A **44**, 3457 (1991).
[27] P. Šeba, Phys. Rev. Lett. **64**, 1855 (1990).
[28] F. Haake, G. Lenz, P. Šeba, J. Stein, H.-J. Stöckmann, and K. Życzkowski, Phys. Rev. A **44**, R6161 (1991).
[29] We evaluate the distribution of intensities for the half-circular billiards numerically. For the rectangular billiards, it is given by $p_{\mathrm{rec}}(I)=1/(\sqrt{I}\pi^2)K(\sqrt{1-I/4})$ with the complete elliptic integral of the first kind K. The Porter-Thomas distribution is $p_{\mathrm{PT}}(I)=1/(\sqrt{2\pi I})e^{-I/2}$.
[30] Performing the averaging over M, we keep the parameter z_0 constant. Since the magnetic field $B=(h/e)n_e z_0/M$ depends on M, B varies. We quantify the magnetic field for $\langle M\rangle$.